



© 2022 The Authors. Gold Open Access: This paper is published under the terms of the CC-BY license.

Manuscript received 14 June 2021 Revised manuscript received 6 September 2021 Manuscript accepted 14 September 2021

Published online 22 November 2021

# Holocene wet episodes recorded by magnetic minerals in stalagmites from Soreg Cave, Israel

Yuval Burstyn<sup>1</sup>, Ron Shaar<sup>1</sup>, Jonathan Keinan<sup>1</sup>, Yael Ebert<sup>1</sup>, Avner Ayalon<sup>2</sup>, Miryam Bar-Matthews<sup>2</sup> and Joshua M. Feinberg<sup>3</sup>

The Institute of Earth Sciences, The Hebrew University of Jerusalem, Jerusalem 91904, Israel <sup>2</sup>Geological Survey of Israel, 32 Yesha'ayahu Leibowitz Street, Jerusalem 9692100, Israel Institute for Rock Magnetism, University of Minnesota, Minneapolis, Minnesota 55455, USA

#### **ABSTRACT**

This study demonstrates the feasibility of speleothem magnetism as a paleo-hydrology proxy in speleothems growing in semi-arid conditions. Soil-derived magnetic particles in speleothems retain valuable information on the physicochemical conditions of the overlying soil, and changes in bedrock hydrology. Yet, the link between magnetic and isotopic proxies of speleothems has been only partly established. We reveal strong coupling between the inflow of magnetic particles (quantified using the magnetic flux index,  $IRM_{flux}$ ) and  $\delta^{13}C$  in two Holocene speleothems from Soreq Cave (Israel). The stalagmite record spans from ca. 9.7 to ca. 5.4 ka, capturing the warm-humid conditions associated with the early Holocene and the transition to mid-Holocene wet-dry cycles. Extremely low IRM<sub>flux</sub> during the early Holocene, indicating minimal contribution from the overlying soil, is accompanied by anomalously high  $\delta^{13}C$  (approaching bedrock values) hypothesized to be caused by high rainfall and soil erosion. By contrast, IRM<sub>flux</sub> during the mid-Holocene covaries with the saw-tooth cyclicity of  $\delta^{13}C$  and  $\delta^{18}O$ , interpreted as rapid fluctuations in rainfall amount. The peaks in IRM<sub>flux</sub> precede the negative (wet)  $\delta^{13}$ C peaks by ~60–120 yr. The apparent lag is explained as a rapid physical translocation of overlying soil particles via groundwater (high  $IRM_{flux}$ ) as a response to increasing rainfall, compared with slower soil organic matter turnover rates (10-10<sup>2</sup> yr).

## INTRODUCTION

Speleothem paleoenvironmental proxy records focus on stable oxygen and carbon isotope time series ( $\delta^{18}$ O and  $\delta^{13}$ C, respectively) (e.g., Fairchild and Baker, 2012; Bar-Matthews et al., 2019). Coupling these data with other climate proxies increases the accuracy and precision of paleoclimate interpretations (Fairchild and Baker, 2012). These other proxies include nontraditional isotopes, trace element geochemistry, and, more recently, mineral magnetism (e.g., Bourne et al., 2015; Zhu et al., 2017). The underlying assumption is that speleothem magnetic properties are controlled by ferromagnetic particles flushed into the cave and encapsulated within calcite laminae (Lascu and Feinberg, 2011). These particles can be detrital in origin (dominated by regionally ubiquitous magnetic minerals such as magnetite, titanomagnetite, and hematite), or authigenic (mainly pedogenic magnetite and goethite) (Lascu and Feinberg, 2011; Bourne et al.,

2015; Jaqueto et al., 2016). The concentration, mineralogy, and size of the magnetic particles can be measured indirectly using non-destructive methods, providing a proxy for the physicochemical properties of the overlying soil and the cave hydrology (Lascu and Feinberg, 2011; Feinberg et al., 2020). However, the interpretation of the magnetic data is not straightforward because the link between climate and magnetic parameters is controlled by the local geohydrology. For example, data from mid-latitude stalagmites suggest that more magnetic particles are delivered into a cave as rainfall increases (e.g., Bourne et al., 2015; Zhu et al., 2017), while the opposite relationship is observed in tropical caves, where magnetic particles are delivered primarily during dry periods (Jaqueto et al., 2016; Fu et al., 2021). Thus, adaptation of speleothem magnetism in paleoclimate models requires a site-specific multiproxy analysis that includes both magnetic and geochemical proxies.

Our study examines the coupling between magnetic parameters and  $\delta^{13}C$  values over centennial to millennial timescales in two Holocene stalagmites from Soreq Cave, Israel (31°45′21″N, 35°01′20″E). The stalagmite record spans the time interval from ca. 9.7 ka to ca. 5.4 ka, with an overlap between ca. 7.0 and ca. 6.4 ka covering the early-Holocene pluvial conditions associated with the deposition of Sapropel layer 1 (S1) in the eastern Mediterranean Sea (Bar-Matthews et al., 2000), followed by the transition to mid-Holocene wet-dry cycles (Bar-Matthews and Ayalon, 2011). We demonstrate the interplay between magnetic and isotopic proxies during regional climate change derived from speleothems deposited under two drip-sites with different hydrochemical settings. This is part of an effort to further develop speleothem magnetism as a standardized paleoenvironmental proxy.

# THE SOREQ CAVE

Soreq Cave (Fig. 1A) is located on the western slopes of the Judean Mountains, 40 km east of the Mediterranean Sea at an elevation of  $\sim$ 400 m above mean sea level. The cave area is ~5000 m<sup>2</sup>, hosted within Cenomanian dolomitic limestone. Bedrock above the cave varies between 10 m to >50 m. The overlying soil occurs as 30–100-cm-thick pockets covering  $\sim$ 50% of the present-day surface (Figure S1 and Section S1 in the Supplemental Material<sup>1</sup>). Flora above the cave are intermingled coniferous forest and C<sub>3</sub> shrubland (Danin, 1992). Mean high annual

rainfall is  $500_{190}^{1034}$  mm with >95% of rain limited to October through May (Ayalon et al., 1998).

Soreq Cave is situated on the boundary between the Mediterranean semi-arid climate zone

Supplemental Material. Extended site description, methods, age model, and results, including data tables. Please visit https://doi.org/10.1130/GEOL.S.16906894 to access the supplemental material, and contact editing@geosociety.org with any questions.

CITATION: Burstyn, Y., et al., 2022, Holocene wet episodes recorded by magnetic minerals in stalagmites from Soreq Cave, Israel: Geology, v. 50, p. 284-288, https://doi.org/10.1130/G49383.1

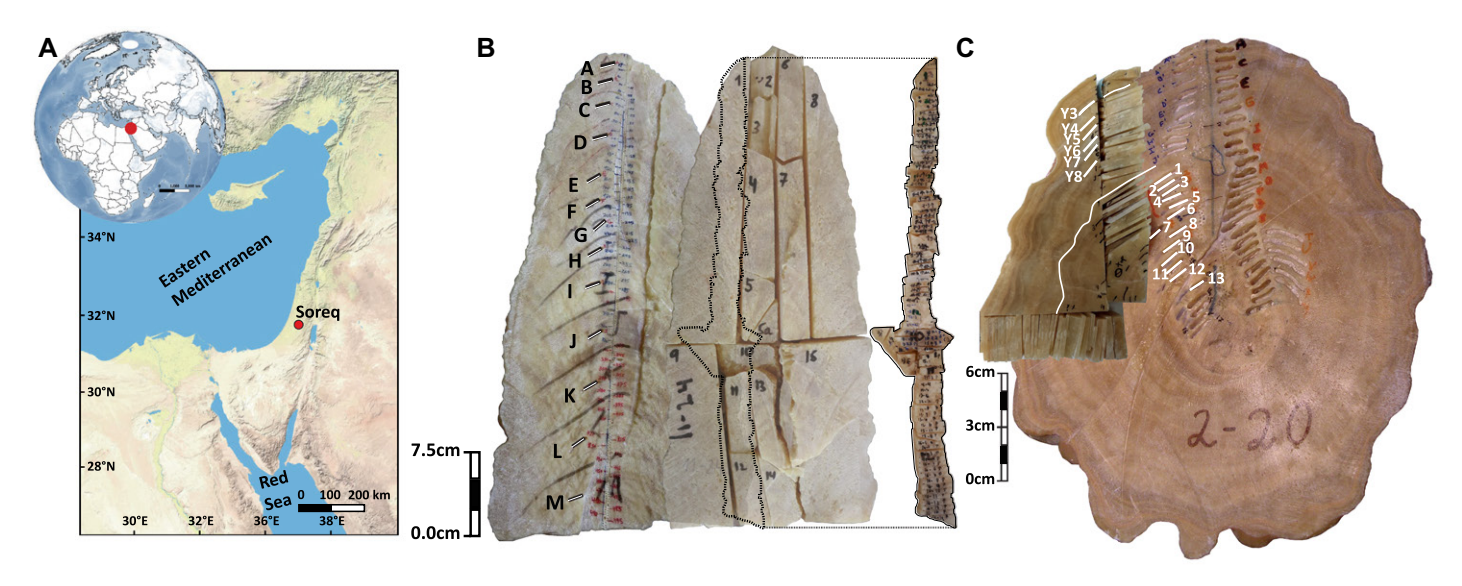


Figure 1. (A) The eastern Mediterranean, with the location of Soreq Cave, Israel (31°45′21″N, 35°01′20″E, WGS84). (B,C) Stalagmites 11-24 and 2-20 superimposed with the slices used for magnetic analysis. Black lines (on 11-24) and white lines (on 2-20) mark the locations of U-Th sampling (denoted by letters and numbers). Small holes (numbered from top to bottom, in intervals of five) mark the stable isotope measurements.

to the north and the arid desert environment to the south, thus acting as a sensitive recorder of changes in hydroclimate and seasonality (Bar-Matthews et al., 2019). The composite isotope record from Soreq secondary calcite speleothems spans ~180 ka and is the quintessential proxy time series for the eastern Mediterranean (Bar-Matthews et al., 2019, and references therein; Section S1 in the Supplemental Material). In addition, Soreq data bracket the timing of the terrestrial occurrence of sapropel S1 (Almogi-Labin et al., 2009) and reveal mid-Holocene wet-dry cycles simultaneous with cultural transitions in the Levant (Bar-Matthews and Ayalon, 2011).

# **METHODS**

Stalagmite 11-24 (from zone 11 in the cave) is a 425-mm-long stalagmite cut along its growth axis. Bar-Matthews and Ayalon (2011) studied one half of the stalagmite for reconstructing paleoclimate, and the second half is used here for paleomagnetic analysis (Fig. 1B; Fig. S2). Stalagmite 2-20 (from zone 2) was cut perpendicular to its growth axis near its base. The ~122-mm-long semi-major axis of the horizontal plane was used for paleoclimate reconstruction (Bar-Matthews et al., 2003; Grant et al., 2012) as well as for paleomagnetic analysis (Fig. 1C, Figs. S2 and S3). The isotopic time series in our study was constructed from 502 drilled samples in stalagmite 11-24 and 162drilled samples in stalagmite 2-20. The agedepth models for the two stalagmites were recalculated with the StalAge R code (Scholz and Hoffmann, 2011; code is available in Comas-Bru et al. [2020]) using 14 of the published U-Th ages from stalagmite 11-24 (Bar-Matthews and Ayalon, 2011) and 16 U-Th ages from stalagmite 2-20 (12 published ages [Grant et al., 2012] and 4 new ages) (Fig. S3; see Section S2 for the age-depth model).

We performed paleomagnetic experiments in the paleomagnetic laboratory at the Institute of Earth Sciences, The Hebrew University of Jerusalem, using a 2G-RAPID cryogenic sample rock magnetometer equipped with in-line AF demagnetization coils and an ASC pulse magnetizer. The samples are thin slices, 2-5 mm thick with a median thickness of 4.2 mm. Stalagmite 11-24 was cut into 82 slices, and stalagmite 2-20 was cut into 44 slices (Figs. 1B and 1C). The samples were washed with distilled water to remove possible contamination from the saw, and a 1.5 T (tesla) DC field was applied to all specimens to amplify the samples' weak natural remanent magnetization (NRM) resulting from a low concentration of magnetic minerals. The isothermal remanent magnetization (IRM) was normalized both to mass (IRM<sub>mass</sub>) and time (IRM<sub>flux</sub>) (Zhu et al., 2017). IRM<sub>mass</sub> is a measure of the relative concentration of magnetic minerals, while  $IRM_{\text{flux}}$  provides the flux of magnetic particles encapsulated in the calcite per unit time, and compensates for growth rate changes. We used coercivity unmixing to characterize the magnetic components in 11 samples: five samples from stalagmite 11-24, three samples from stalagmite 2-20, two samples from the overlying Terra Rossa Mediterranean soil (at depths of 5 and 30 cm), and one sample from clay collected inside the cave. The procedure included 95 alternating field (AF) demagnetization steps from 1 mT to 250 mT after applying the 1.5 T field. Unmixing data were analyzed using the MAX UnMix program (Egli, 2004; Maxbauer et al., 2016).

A  $2 \times 3$  cm slice cut from the middle of stalagmite 11-24 (Fig. 1B) was used for electron microscopy using an extreme high resolution

scanning electron microscope (XHR-SEM; Magellan 400L). The slice was cleaned but not polished, to preserve the magnetic particles occurring between calcite crystals. See Section S3 of the Supplemental Material for the extended methods.

#### ORIGIN OF MAGNETIC PARTICLES

Electron microscopy coupled with energy dispersive spectroscopy (EDS) analysis shows the presence of 0.5  $\mu m$  to  $\sim 2 \mu m$  anhedral ferromagnetic grains occurring at the interstices of speleothem calcite grains (Fig. S5). The morphology of the sub-micrometer particles resembles pedogenic magnetite (Strauss et al., 2013), where the larger ones may be weathered detrital particles. Coercivity spectra of the stalagmites samples (Fig. S6a) broadly agree with values reported in previously published speleothem studies (Lascu and Feinberg, 2011; Osete et al., 2012; Bourne et al., 2015; Zhu et al., 2017) and are in the range of pedogenic and detrital magnetite (Egli, 2004). The IRM unmixing data, interpreted with two end-member populations (high-coercivity [HC; median destructive field, MDF, >25 mT] and low-coercivity [LC; MDF <15 mT]), show a general agreement between the stalagmites, the overlying soil, and the clay material found in the cave. The contribution of the HC component in the soil and the clay is lower than that of the stalagmites (Section S2 and Table S2), indicating that the grains incorporated into stalagmites were filtered toward smaller grain sizes when infiltrating through the karst. The IRM unmixing of local dolomite bedrock, characterized by a weak IRM of  $<10^{-7}$  Am<sup>2</sup>, revealed a significant (30%-50%) component with much higher coercivity (>250 mT), which could not be fully demagnetized with standard AF methods (Fig. S6b). This dolomite-driven component is not incorporated in the stalagmites. Our observations support the underlying assumption that the magnetic minerals in the speleothems are micrometer- to sub-micrometer-sized particles derived from overlying soil and filtered through the karst system.

#### MAGNETO-ISOTOPIC TIME SERIES

The interval spanning ca. 9.7 to ca. 5.4 ka (Fig. 2) includes the absolute maxima and minima in the entire Holocene  $\delta^{13}$ C and  $\delta^{18}$ O records of Soreq (Bar-Matthews et al., 2019), representing the most extreme climate variations of the interglacial. Inspection of the overlap-

ping time series between ca. 7.0 and ca. 6.4 ka shows that IRM<sub>mass</sub> values of stalagmite 2-20 are approximately half an order of magnitude higher than those of stalagmite 11-24 (Fig. 2E). This difference is explained by the drip site–specific, nonlinear nature of karst hydrology (Treble et al., 2013) associated with the stalagmites that formed in different parts of the cave (Fig. S2). Specifically, the geochemical model for Soreq Cave (Burstyn, 2013; Section S1) estimates a higher fraction of soil-derived elements and a significant fraction of vadose flow in the shallower locations, where stalagmite 2-20 was formed. By contrast, IRM<sub>flux</sub> values of the two

stalagmites are within the same value range, and their mean IRM $_{\text{flux}}$  is indistinguishable within  $1\sigma$  uncertainty. This suggests that IRM $_{\text{flux}}$  is a potential normalized index for comparing multiple samples from the same cave (Section S4 and Tables S3–S6).

#### EARLY-HOLOCENE WET PERIOD

The early-Holocene recorded in stalagmite 2-20 is marked by a rapid decrease in IRM<sub>flux</sub> to minimum Holocene values (Fig. 2D). The low IRM<sub>flux</sub> coincides with a distinct isotopic event between ca. 9.5 and ca. 7.1 ka, where  $\delta^{13}$ C values are uniquely high (-8% to -4%; Fig. 2C)

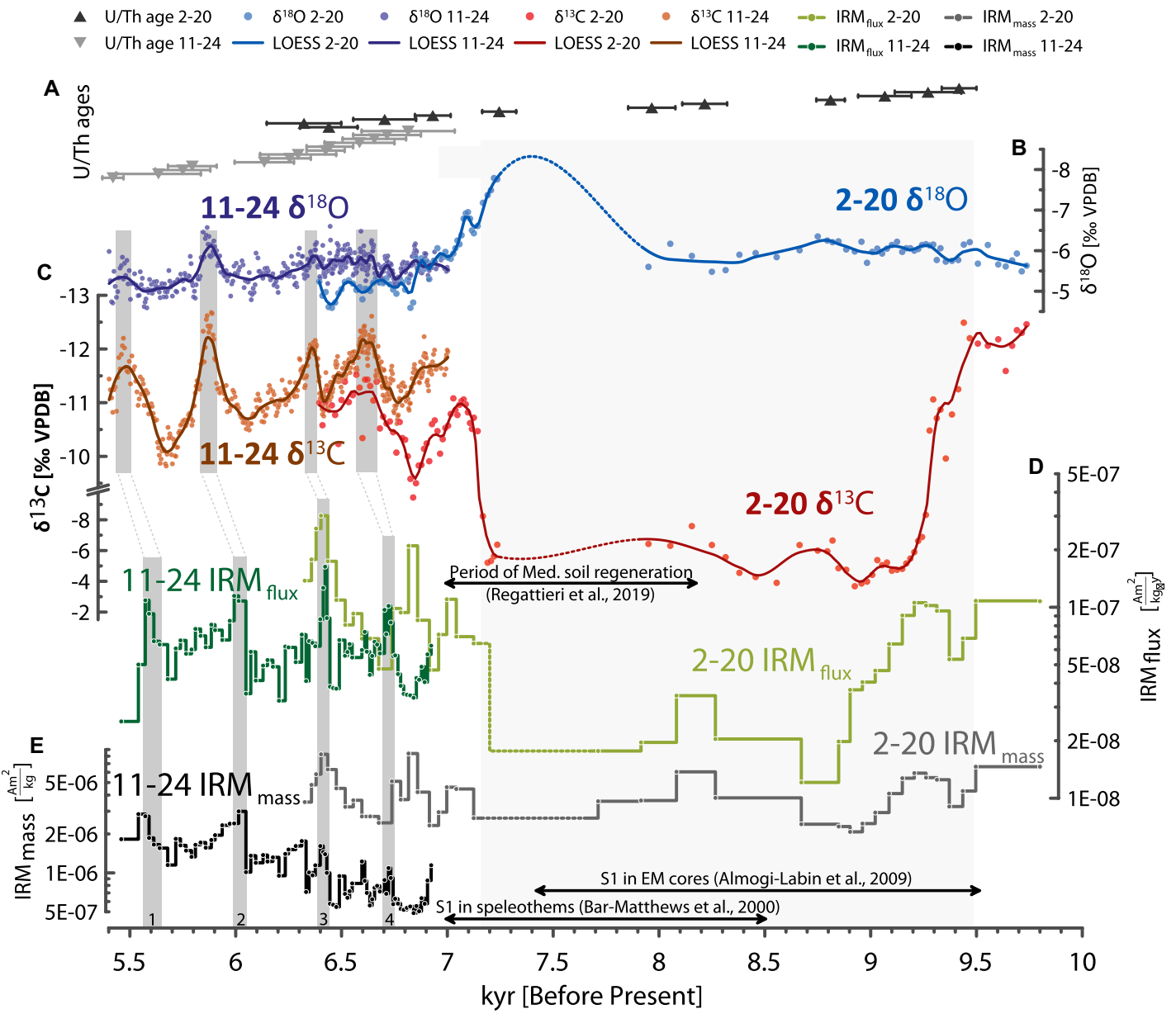


Figure 2. Composite multi-proxy time series of stalagmites 2-20 and 11-24 from Soreq Cave, Israel. (A) U-Th ages used for the age model. (B,C)  $\delta^{18}$ O and  $\delta^{13}$ C time series superimposed with a locally estimated scatterplot smoothing (LOESS) function with a Gaussian kernel and second-order locally weighted polynomial. Light gray shaded area is the isotopic excursion defining sapropel layer S1. Dark-gray vertical bands in C and E highlight four mid-Holocene wet-dry cycles (see text for details). VPDB—Vienna Peedee belemnite. (D,E) Isothermal remanent magnetization normalized to flux (IRM<sub>flux</sub>) and to mass (IRM<sub>mass</sub>). Sapropel 1 (S1) timing is marked by black arrowed lines in E and by light-gray shading throughout the plot. Timing of Mediterranean (Med.) soil regeneration in D is marked by black arrowed line (Regattieri et al. (2019).

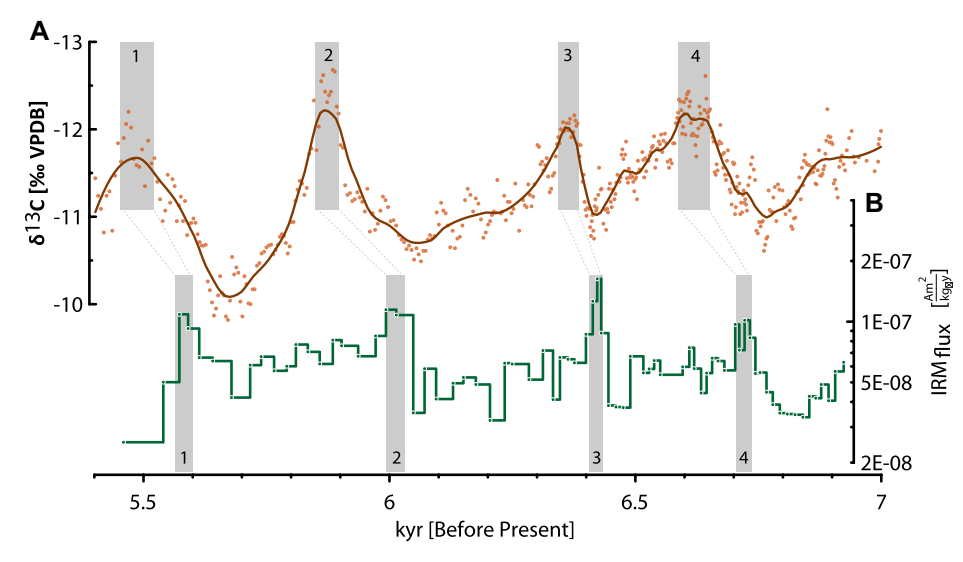


Figure 3. Correlation between  $\delta^{13}C$  (A) and isothermal remanent magnetization normalized to flux (IRM<sub>flux</sub>) (B) in stalagmite 11-24 from Soreq Cave, Israel during mid-Holocene wet-dry cycles. Cycles are highlighted here by dark-gray vertical bands numbered 1 through 4. Colors of dots and lines are as in Figure 2. VPDB—Vienna Peedee belemnite.

relative to the Soreq overall mean, approaching bedrock values of 2% (Section S1). Conversely, the termination of early-Holocene conditions is observed between ca. 7.2 ka and ca. 7.1 ka as stalagmite 2-20 δ<sup>13</sup>C values decreased back to  $C_3$ -like values (-10% to -12%), simultaneous with IRM<sub>flux</sub> returning to pre-sapropel values (Figs. 2C and 2D). This excursion in the stalagmite record corresponds with sapropel layer S1 in the eastern Mediterranean sea (striped gray bar in Fig. 2), thought to be warm and humid (Nehme et al., 2015; Bar-Matthews et al., 2019; Goldstein et al., 2020). Bar-Matthews et al. (2003) explained the  $\delta^{13}$ C excursion as meteoric water reaching the cave after little interaction with overlying soil due to either (1) recently eroded soils, as water percolating through minimal soil cover will be undersaturated in low- $\delta^{13}$ C soil CO<sub>2</sub> (Genty et al., 2001), or (2) high runoff fraction, circumventing the soil pathway altogether. Both hypotheses are supported by a coeval drop in 87Sr/86Sr and initial (234U/238U) ratios toward bedrock ratios (Ayalon et al., 1999). The IRM<sub>flux</sub> as a soil contribution proxy may help differentiate between these hypotheses.

Thus, the entire early Holocene is bracketed between the ca. 9.5 ka weakening of the soil-related isotopic component and the large decrease in IRM<sub>flux</sub>, followed by the ca. 7.1 ka rehabilitation of the  $C_3$  isotopic signal and IRM<sub>flux</sub> values, which is coupled with evidence of soil regeneration in the circum-Mediterranean region (Regattieri et al., 2019). We believe that the structure of the low-IRM<sub>flux</sub> event (rapid decrease/increase) and the regional evidence of soil regeneration in the termination of that event supports the hypothesis that a change in soil cover or soil stability resulted in a change in  $\delta^{13}$ C (and IRM<sub>flux</sub>) values. Apparently, the post-glacial

increase in rainfall destabilized soils, perhaps coupled with a "shut down" of soil production due to a decrease in dust input during the "green Sahara" phase (see Rohling et al., 2015).

#### MID-HOLOCENE WET-DRY CYCLES

The post-sapropel mean IRM<sub>flux</sub> values suggest that the soil overlying Soreq Cave was regenerated and stabilized by the mid-Holocene. The four saw-tooth cycles in IRM<sub>flux</sub> between ca. 7.0 and ca. 5.4 ka (numbered in Figures 2E and 3) are also evident in the  $\delta^{13}$ C and  $\delta^{18}$ O records (Section S4). These cycles were attributed to wet-dry events (Mayewski et al., 2004; Bar-Matthews and Ayalon, 2011). Bar-Matthews and Ayalon (2011) interpreted low  $\delta^{18}$ O values as an increase in regional rainfall superimposed with strong annual variations, while the  $\delta^{13}$ C cyclicity was smoothed and amplified by complex soil processes, as they represent changes in soil organic carbon. Thus, the post-sapropel regeneration of soil is linked to the emergence of a positive relationship between IRM<sub>flux</sub> and rainfall amount, as also observed in other midlatitude sites (Zhu et al., 2017; Regattieri et al., 2019; Feinberg et al., 2020).

The mid-Holocene record also highlights an apparent phase shift between the physical flux of magnetic particles into Soreq Cave and the chemical processes affecting the  $\delta^{13}$ C of drip water (Fig. 3). The IRM<sub>flux</sub> peaks precede  $\delta^{13}$ C minima by  $\sim$ 60 to 120 yr, where a maximum correlation factor between the two records is achieved by a time-shift of 60 yr (Fig. S7). This lag can be explained by the mechanisms governing the two proxies: (1) An increase in rainfall typically results in increased production of pedogenic magnetic minerals (Maxbauer et al., 2017, and references within) simultaneously en-

hancing physical flushing of soil particles into the cave. (2) In contrast, the change in soil water content, temperature, vegetation cover, and soil activity that affect biogenic soil- $CO_2$  concentrations may require several decades to develop and affect  $\delta^{13}C$  values (Genty et al., 2001). Another hypothesis is that a rise in rainfall increases vegetation cover to a certain threshold, inhibiting transfer of fine-grained magnetite (e.g., Chen et al., 2019) and increasing the time lag between peak values of each proxy.

## **CONCLUSIONS**

Soreq Cave demonstrates two opposite responses of the magnetic flux parameter to increasing rainfall. During the early-Holocene, low-IRM<sub>flux</sub> and high-δ<sup>13</sup>C indicate minimal contribution from soils, adding to the isotopicbased hypothesis of soil removal and regeneration during the prevailing warm-humid climate conditions of sapropel S1 (e.g., Goldstein et al., 2020). During the mid-Holocene, couplets of high-IRM<sub>flux</sub> and low- $\delta^{13}$ C are associated with increased precipitation of wet-dry cycles. A phase shift between the couplets may elucidate soil and vegetation dynamics, crucial to interpreting subannual-resolution climate data (e.g., Orland et al., 2014). We show that IRM<sub>flux</sub> in speleothems is a valuable proxy for regional changes in soil-related processes.  $IRM_{\text{flux}}$  could be used to resolve controversies in interpreting the complex behavior of isotopes in geological records, and could hold the potential to constrain soil carbon turnover response to climate events.

## ACKNOWLEDGMENTS

This research was supported by the U.S.—Israel Bi-National Science Fund grant #2016402, the U.S. National Science Foundation grant EAR-2044535, and the European Research Council Horizon 2020 research and innovation program, agreement No. 804490. We thank V. Gutkin for his help with SEM analysis, and L. Comas-Bru and M. Deininger for their comments. We thank three anonymous reviewers and K. Benison for their constructive reviews.

## REFERENCES CITED

Almogi-Labin, A., Bar-Matthews, M., Shriki, D., Kolosovsky, E., Paterne, M., Schilman, B., Ayalon, A., Aizenshtat, Z., and Matthews, A., 2009, Climatic variability during the last ~90 ka of the southern and northern Levantine Basin as evident from marine records and speleothems: Quaternary Science Reviews, v. 28, p. 2882–2896, https://doi.org/10.1016/j.quascirev.2009.07.017.

Ayalon, A., Bar-Matthews, M., and Sass, E., 1998, Rainfall-recharge relationships within a karstic terrain in the Eastern Mediterranean semi-arid region, Israel: δ<sup>18</sup>O and δD characteristics: Journal of Hydrology (Amsterdam), v. 207, p. 18–31, https://doi.org/10.1016/S0022-1694 (98)00119-X.

Ayalon, A., Bar-Matthews, M., and Kaufman, A., 1999, Petrography, strontium, barium and uranium concentrations, and strontium and uranium isotope ratios in speleothems as palaeoclimatic proxies: Soreq Cave, Israel: The Holocene, v. 9, p. 715–722, https://doi.org/10.1191/095968399 673664163.

- Bar-Matthews, M., and Ayalon, A., 2011, Mid-Holocene climate variations revealed by high-resolution speleothem records from Soreq Cave, Israel and their correlation with cultural changes: The Holocene, v. 21, p. 163–171, https://doi.org/10.1177/0959683610384165.
- Bar-Matthews, M., Ayalon, A., and Kaufman, A., 2000, Timing and hydrological conditions of Sapropel events in the Eastern Mediterranean, as evident from speleothems, Soreq Cave, Israel: Chemical Geology, v. 169, p. 145–156, https:// doi.org/10.1016/S0009-2541(99)00232-6.
- Bar-Matthews, M., Ayalon, A., Gilmour, M.A., Matthews, A., and Hawkesworth, C.J., 2003, Sea-land oxygen isotopic relationships from planktonic foraminifera and speleothems in the Eastern Mediterranean region and their implication for paleorainfall during interglacial intervals: Geochimica et Cosmochimica Acta, v. 67, p. 3181–3199, https://doi.org/10.1016/S0016-7037(02)01031-1.
- Bar-Matthews, M., Keinan, J., and Ayalon, A., 2019, Hydro-climate research of the late quaternary of the Eastern Mediterranean–Levant region based on speleothems research—A review: Quaternary Science Reviews, v. 221, p. 105872, https://doi .org/10.1016/j.quascirev.2019.105872.
- Bourne, M.D., Feinberg, J.M., Strauss, B.E., Hardt, B., Cheng, H., Rowe, H.D., Springer, G., and Edwards, R.L., 2015, Long-term changes in precipitation recorded by magnetic minerals in speleothems: Geology, v. 43, p. 595–598, https://doi.org/10.1130/G36695.1.
- Burstyn, Y., 2013, Multi-decade to Seasonal Climate Change Recorded by Stable Isotope and Trace Element Variability in Modern Cave-waters and Calcite of Soreq Cave, Israel:, Geological Survey of Israel Report GSI/13/2013, 86 p.
- Chen, Q., Zhang, T.W., Wang, Y.T., Zhao, J.X., Feng, Y.X., Liao, W., Wang, W., and Yang, X.Q., 2019, Magnetism signals in a stalagmite from southern China and reconstruction of paleorainfall during the interglacial-glacial transition: Geophysical Research Letters, v. 46, https://doi org/10.1029/2019GL082204.
- Comas-Bru, L., et al., 2020, SISALv2: A comprehensive speleothem isotope database with multiple age-depth models: Earth System Science Data, v. 12, p. 2579–2606, https://doi.org/10.5194/essd-12-2579-2020.
- Danin, A., 1992, Flora and vegetation of Israel and adjacent areas: Bocconea, v. 3, p. 18–42.
- Egli, R., 2004, Characterization of individual rock magnetic components by analysis of remanence curves:

  1. Unmixing natural sediments: Studia Geophysica et Geodaetica, v. 48, p. 391–446, https://doi.org/10.1023/B:SGEG.0000020839.45304.6d.
- Fairchild, I.J., and Baker, A., 2012, Speleothem Science: From Process to Past Environments: New York, John Wiley & Sons, volume 3, 432 p., https://doi.org/10.1002/9781444361094.

- Feinberg, J.M., Lascu, I., Lima, E.A., Weiss, B.P., Dorale, J.A., Alexander, E.C., and Edwards, R.L., 2020, Magnetic detection of paleoflood layers in stalagmites and implications for historical land use changes: Earth and Planetary Science Letters, v. 530, 115946, https://doi.org/10.1016/j.epsl.2019.115946.
- Fu, R.R., Hess, K., Jaqueto, P.F., Novello, V.F., Kukla, T., Trindade, R.I.F., Stríkis, N.M., Cruz, F.W., and Ben Dor, O., 2021, High-resolution environmental magnetism using the Quantum Diamond Microscope (QDM): Application to a tropical speleothem: Frontiers of Earth Science, v. 8, p. 674, https://doi.org/10.3389/feart.2020.604505.
- Genty, D., Baker, A., Massault, M., Proctor, C., Gilmour, M., Pons-Branchu, E., and Hamelin, B., 2001, Dead carbon in stalagmites: Carbonate bedrock paleodissolution vs. ageing of soil organic matter. Implications for <sup>13</sup>C variations in speleotherms: Geochimica et Cosmochimica Acta, v. 65, p. 3443–3457, https://doi.org/10.1016/ S0016-7037(01)00697-4.
- Goldstein, S.L., Kiro, Y., Torfstein, A., Kitagawa, H., Tierney, J., and Stein, M., 2020, Revised chronology of the ICDP Dead Sea deep drill core relates drier-wetter-drier climate cycles to insolation over the past 220 kyr: Quaternary Science Reviews, v. 244, p. 106460, https://doi .org/10.1016/j.quascirev.2020.106460.
- Grant, K.M., Rohling, E.J., Bar-Matthews, M., Ayalon, A., Medina-Elizalde, M., Ramsey, C.B., Satow, C., and Roberts, A.P., 2012, Rapid coupling between ice volume and polar temperature over the past 50,000 years: Nature, v. 491, p. 744–747, https://doi.org/10.1038/nature11593.
- Jaqueto, P.F., Trindade, R.I.F., Hartmann, G.A., Novello, V.F., Cruz, F.W., Karmann, I., Strauss, B.E., and Feinberg, J.M., 2016, Linking speleothem and soil magnetism in the Pau d'Alho cave (central South America): Journal of Geophysical Research: Solid Earth, v. 121, p. 7024–7039, https://doi.org/10.1002/2016JB013541.
- Lascu, I., and Feinberg, J.M., 2011, Speleothem magnetism: Quaternary Science Reviews, v. 30, p. 3306–3320, https://doi.org/10.1016/j.quascirev.2011.08.004.
- Maxbauer, D.P., Feinberg, J.M., and Fox, D.L., 2016, MAX UnMix: A web application for unmixing magnetic coercivity distributions: Computers & Geosciences, v. 95, p. 140–145, https://doi .org/10.1016/j.cageo.2016.07.009.
- Maxbauer, D.P., Feinberg, J.M., Fox, D.L., and Nater, E.A., 2017, Response of pedogenic magnetite to changing vegetation in soils developed under uniform climate, topography, and parent material: Scientific Reports, v. 7, p. 1–10, https://doi.org/10.1038/s41598-017-17722-2.
- Mayewski, P.A., et al., 2004, Holocene climate variability: Quaternary Research, v. 62, p. 243–255, https://doi.org/10.1016/j.yqres.2004.07.001.

- Nehme, C., Verheyden, S., Noble, S.R., Farrant, A.R., Sahy, D., Hellstrom, J.C., Delannoy, J.J., and Claeys, P., 2015, Reconstruction of MIS 5 climate in the central Levant using a stalagmite from Kanaan Cave, Lebanon: Climate of the Past, v. 11, p. 1785– 1799, https://doi.org/10.5194/cp-11-1785-2015.
- Orland, I.J., Burstyn, Y., Bar-Matthews, M., Kozdon, R., Ayalon, A., Matthews, A., and Valley, J.W., 2014, Seasonal climate signals (1990–2008) in a modern Soreq Cave stalagmite as revealed by high-resolution geochemical analysis: Chemical Geology, v. 363, p. 322–333, https://doi.org/10.1016/j.chemgeo.2013.11.011.
- Osete, M.L., Martín-Chivelet, J., Rossi, C., Edwards, R.L., Egli, R., Muñoz-García, M.B., Wang, X., Pavón-Carrasco, F.J., and Heller, F., 2012, The Blake geomagnetic excursion recorded in a radiometrically dated speleothem: Earth and Planetary Science Letters, v. 353–354, p. 173–181, https://doi.org/10.1016/j.epsl.2012.07.041.
- Regattieri, E., et al., 2019, Holocene Critical Zone dynamics in an Alpine catchment inferred from a speleothem multiproxy record: disentangling climate and human influences: Scientific Reports, v. 9, p. 17829, https://doi.org/10.1038/s41598-019-53583-7.
- Rohling, E.J., Marino, G., and Grant, K.M., 2015, Mediterranean climate and oceanography, and the periodic development of anoxic events (sapropels): Earth-Science Reviews, v. 143, p. 62–97, https://doi.org/10.1016/j.earscirev.2015.01.008.
- Scholz, D., and Hoffmann, D.L., 2011, StalAge— An algorithm designed for construction of speleothem age models: Quaternary Geochronology, v. 6, p. 369–382, https://doi.org/10.1016/j.quageo.2011.02.002.
- Strauss, B.E., Strehlau, J.H., Lascu, I., Dorale, J.A., Penn, R.L., and Feinberg, J.M., 2013, The origin of magnetic remanence in stalagmites: Observations from electron microscopy and rock magnetism: Geochemistry Geophysics Geosystems, v. 14, p. 5006–5025, https://doi .org/10.1002/2013GC004950.
- Treble, P.C., Bradley, C., Wood, A., Baker, A., Jex, C.N., Fairchild, I.J., Gagan, M.K., Cowley, J.A., and Azcurra, C., 2013, An isotopic and modelling study of flow paths and storage in Quaternary calcarenite, SW Australia: Implications for speleothem paleoclimate records: Quaternary Science Reviews, v. 64, p. 90–103, https://doi .org/10.1016/j.quascirev.2012.12.015.
- Zhu, Z., Feinberg, J.M., Xie, S., Bourne, M.D., Huang, C., Hu, C., and Cheng, H., 2017, Holocene EN-SO-related cyclic storms recorded by magnetic minerals in speleothems of central China: Proceedings of the National Academy of Sciences of the United States of America, v. 114, p. 852–857, https://doi.org/10.1073/pnas.1610930114.

Printed in USA